Multiparticle-rotor model for rotational band structure of ^{154}Gd

S. Y. Chu, J. O. Rasmussen, and M. A. Stoyer
Lawrence Berkeley National Laboratory, Berkeley, California 94720

P. Ring
Technische Universität München, D-85748 Garching, Germany

L. F. Canto
Universidade Federal do Rio de Janeiro, C.P. 68528, 21945 Rio de Janeiro, Rio de Janeiro, Brazil
(Received 23 June 1994; revised manuscript received 25 April 1995)

Band-crossing phenomena in the high-spin region of deformed nuclei are studied in this paper. The power of modern computers for large-matrix diagonalization (up to 17 527×17 527) is exploited in a multinucleon-plus-rotor model. The interesting test case of ^{154}Gd is treated in this paper. Though a small basis set of 9–18 Nilsson orbitals is used, the strict angular momentum and particle number conservation guarantees superior orthogonal microscopic wave functions for nucleon transfer calculations. This method takes account of pairing correlations among the valence particles and shows the effects of quadrupole pairing and the usually neglected $\mathbf{j}\cdot\mathbf{j}$ recoil terms.

PACS number(s): 21.10.Re, 21.60.eV, 27.70.+q

I. INTRODUCTION

The "backbending" phenomenon for yrast lowest bands of spheroidal even-even nuclei has drawn much attention since its discovery [1]. It was first thought to signal the rotation-induced pairing collapse ("the nuclear Meissner effect") predicted by Mottelson and Valatin [2]. Later, the general explanation shifted to a spin alignment of some high-j neutron orbitals, an explanation which was proposed and modeled first by Stephens and Simon [3]. In this picture there is a crossing of the ground band with a spin-aligned band at some spin, which happens around $(12-18)\hbar$ in the rare-earth region. Bengtsson, Hamamoto, and Mottelson [4] showed, after correcting a phase factor in Ref. [3], that the mixing matrix element between these two bands varies sinusoidally as the chemical potential moves through the $i_{13/2}$ neutron subshell. The mixing strength V_I moves through zero when the chemical potential is slightly above one of the $i_{13/2}$ Nilsson levels other than the first or last. When the chemical potential of a real nucleus is near a zero of the mixing matrix element, the band crossing is sharp. When the chemical potential is midway between zeros, the band crossing is soft.

Many refined models, too numerous to mention in this Introduction, have been applied over the intervening years. Many of these models are based on variational wave functions and quasiparticle formalisms in which either angular momentum or particle number or both fluctuate. These variational methods have difficulties with excited states.

Thus, it seemed important to expand on a more conventional deformed shell model strictly conserving particle number and angular momentum. Furthermore, this approach could be more reliable for the excited band structure of deformed nuclei. Shell-model calculations for several valence particles coupled to a rotor were carried out in the past only allowing particles in one intruder shell [5]. Engeland [6] has used Hamiltonian matrix diagonalization to calculate such solutions for deformed nuclei. His diagonalization used a two-step procedure: First diagonalize within each K subspace, and then mix the K solutions with the Coriolis force. Our Hamiltonian matrix diagonalization (HMD) method solves the matrix in a single step. This has the advantage that it is easy to calculate the matrix elements, and the resultant matrix is sparse and can be efficiently diagonalized by the LANCZOS algorithm for the lowest few eigenstates. In earlier model studies, some of the authors of this paper calculated seniority-0 even-even 0^+ states by exact matrix diagonalization of a pairing-force Hamiltonian with a half-filled, uniform level spacing in a six-Nilsson-orbital system [7]. Later we treated a set of nine orbitals about the chemical potential [8]. In the present work we extend the method to include nonzero even-spin values. We showed a first application of these methods to even-even thorium isotopes [9], though without quadrupole pairing. The material of this present paper is mostly from the thesis of one of us [10]. In Sec. II, the Hamiltonian is discussed. In Sec. III, the choice of basis states is discussed. In Sec. IV, energy level results and other properties of separate neutron and proton systems are shown and discussed. In Sec. V, the results for the very large matrices of combined proton and neutron systems are shown and discussed. In Sec. VI is a general discussion and conclusions. Appendix A contains details on input parameters and Appendix B has results of calculations at larger quadrupole deformation than those in the main text.

II. HAMILTONIAN

The Hamiltonian can be written

$$\mathbf{H}=\mathbf{H}_{\rm SP}+\mathbf{H}_{gm}+\mathbf{H}_{gq}+\mathbf{H}_{\rm rot}, \tag{1}$$

where

$$\mathbf{H}_{\mathrm{SP}} = \sum_{\nu} \epsilon_{\nu} \mathbf{a}^{\dagger}_{\nu} \mathbf{a}_{\nu}, \tag{2}$$

$$\mathbf{H}_{gm} = G_m \sum_{\nu_1,\nu_2>0} \mathbf{a}^{\dagger}_{\nu_1} \mathbf{a}^{\dagger}_{\bar{\nu}_1} \mathbf{a}_{\bar{\nu}_2} \mathbf{a}_{\nu_2}, \tag{3}$$

$$\mathbf{H}_{gq} = G_q \left\{ \left(\sum_{|\mu|\leq 2} \mathbf{P}^{\dagger}_{2\mu} \mathbf{P}_{2\mu} \right) - \mathbf{S} \right\} . \tag{4}$$

The definition of $\mathbf{H}$ in Eq. (1) corresponds to Eq. (4.135) of Ring and Schuck [11] except for the radial integral, which is taken here as unity. The quadrupole pair creation operator $\mathbf{P}^{\dagger}_{2\mu}$ is defined as follows:

$$\mathbf{P}^{\dagger}_{2\mu} = \frac{1}{2} \sum_{\nu_1,\nu_2} \langle \nu_1 \mid Y_{2\mu} \mid -\nu_2 \rangle \mathbf{a}^{\dagger}_{\nu_1} \mathbf{a}^{\dagger}_{\nu_2} . \tag{5}$$

In Eqs. (2)–(5), $\mathbf{a}^{\dagger}_{\nu}$ and $\mathbf{a}^{\dagger}_{\bar{\nu}}$ are, respectively, creation operators for the single-particle state ν and its time-reversal conjugate $\bar{\nu}$. In the quadrupole-pairing term, the diagonal self-energy contribution $\mathbf{S}$, where

$$\mathbf{S} = \sum_{\nu} |\langle \nu \mid Y_{20} \mid \bar{\nu} \rangle|^2 a^{\dagger}_{\nu} a^{\dagger}_{\bar{\nu}} a_{\bar{\nu}} a_{\nu} , \tag{6}$$

is subtracted, since it would introduce unphysical energy shifts in selected single-particle orbitals. The rotational term $\mathbf{H}_{\mathrm{rot}}$ will be discussed later in the section.

The single-particle Hamiltonian is that of Cwiok *et al.* [13] for the deformed Woods-Saxon potential, including quadrupole and hexadecapole deformations. For details, see Appendix A.

Both monopole and quadrupole pairing are included in the calculation. Our combined pairing strength (G_m and G_q) is adjusted so the gap at low spin to noncollective excited bands is about twice the experimental odd-even mass difference, as determined by a spline fit to the masses of the gadolinium isotopes with $N=89$–94. Relative matrix elements of quadrupole pairing were estimated from the slopes of orbitals in the deformed Woods-Saxon energy plots (Figs. 6 and 7, below).

It is, at first, not obvious how to adjust the strength of the quadrupole pairing relative to that of the monopole. A ratio of unity in our units (0.25 in units of Ref. [14]) would correspond to a surface delta force, quite similar to the density-dependent delta interaction, successfully used in deformed nuclei by Chasman [12]. Hara and Sun [14] used a somewhat weaker ratio G_q/G_m of 70% of the surface delta interaction values. There are three components of quadrupole pairing: Y_{20}, Y_{21}, and Y_{22}. Hamamoto [15] has pointed out the possible importance of the Y_{21} component in microscopic calculations of the moment of inertia. The Y_{20} component plays a special role in a region of the Nilsson diagram where the orbitals fall into two families, downgoing (prolate driving) and upgoing (oblate driving) (see Appendix A). The quadrupole interaction strengthens pairing between orbitals with similar slopes but weakens it between orbitals with strongly differing slopes, much as a short-range or delta function would weaken the interaction between orbitals with little overlap. The 90-neutron isotones are just over the borderline for stabilized deformed ground states, with $N\leq 88$ generally having on average spherical ground states. This fairly sharp demarcation is in part a consequence of there being, in addition to several downgoing orbitals, strongly upgoing (oblate) $h_{11/2}$ orbitals very near the Fermi surface. The even-Z 90-neutron isotones generally have unusually low excited 0^+ bands ($\sim$ 600–800 keV). We find that the energy of these excited 0^+ bands is quite sensitive to the G_q/G_m ratio in the calculation. Thus, we renormalize the Y_{20} part of the quadrupole pairing to a high ratio ($\sim$ 2.5) to fit the $0^{+\prime}$ energy (a larger configuration space with more orbitals would not require such a large renormalization of the Y_{20} quadrupole pairing). The Y_{21} and Y_{22} components of quadrupole pairing are left at their delta-force strength. This means in particular that the residual interaction used in this investigation is no longer rotationally invariant. Since our forces are effective forces in the intrinsic scheme, where rotational symmetry is broken anyhow, this fact does not hurt the final rotational invariance of our total wave function, which is guaranteed by the coupling to the rotor.

The rotational energy part of the Hamiltonian is treated with more care than usual. Bohr [16], in 1951, gave the expression for the rotational energy associated with a single nucleon strongly coupled to a spheroidal core, and this expression is usually used for the diagonal rotational energy in odd-A nuclei before Coriolis mixing of states. If one derives the expression for core rotational energy with more than one nucleon, new terms of the form $\mathbf{j}\cdot\mathbf{j}$ appear. Let the rotor angular momentum be $\mathbf{R}$, then,

$$\mathbf{R} = \mathbf{I} - \sum_{\nu_1\nu_2} \langle \nu_2 \mid \mathbf{j} \mid \nu_1 \rangle \mathbf{a}^{\dagger}_{\nu_2} \mathbf{a}_{\nu_1}. \tag{7}$$

If the body-fixed coordinates are labeled by x', y', and z', where z' is the cylindrical symmetry axis, then the rotational Hamiltonian can be expressed as follows:

$$\mathbf{H}_{\mathrm{rot}} \equiv a_{\mathrm{rot}} (\mathbf{R}^2_{x'} + \mathbf{R}^2_{y'}) \tag{8}$$

$$= a_{\mathrm{rot}} \left[(\mathbf{I}^2 - \mathbf{I}^2_{z'}) - \sum_{\nu_1\nu_2} [\mathbf{I}_+ (j_-)_{\nu_2\nu_1} + \mathbf{I}_- (j_+)_{\nu_2\nu_1}] \mathbf{a}^{\dagger}_{\nu_2} \mathbf{a}_{\nu_1} \right] + a_{\mathrm{rot}} \mathbf{H}_{jj}, \tag{9}$$

where $(j_{\pm})_{\nu_1\nu_2}$ and $\mathbf{H}_{jj}$ are

$$(j_{\pm})_{\nu_2\nu_1} \equiv \langle \nu_2 \mid \mathbf{j}_{\pm} \mid \nu_1 \rangle \equiv \langle \nu_2 \mid \mathbf{j}_{x'} \pm i\, \mathbf{j}_{y'} \mid \nu_1 \rangle \tag{10}$$

TABLE I. Input parameters for various calculations.

	9 proton levels	9 neutron levels	12 neutron levels	12 neutron levels	9 proton and 9 neutron levels	
β_2	0.23	0.23	0.23	0.28	0.23	
$a_{\rm rot}(0)$ (MeV/$\hbar^2$)	0.017	0.019	0.019	0.019	0.024	
$a'_{\rm rot}$ ($\hbar^{-2}$)	0.002	0.002	0.002	near constant	0.002	
	P	N	N	N	P	N
G_m (MeV)	0.355	0.29	0.24	0.24	0.37	0.33
G_q	0.355	0.29	0.24	0.24	0.37	0.33
G_q for Y_{20}	0.888	0.73	0.60	0.72	0.92	0.83
Particle number	10	8	10	12	10	8

and

$$\mathbf{H}_{jj}=\frac{1}{2}\sum_{\nu_1\nu_2}\left[\sum_{\nu}\left[(j_+)_{\nu_2\nu}(j_-)_{\nu\nu_1}+(j_+)_{\nu\nu_1}(j_-)_{\nu_2\nu}\right]\right]\mathbf{a}^\dagger_{\nu_2}\,\mathbf{a}_{\nu_1}$$
$$-\sum_{\substack{\nu_1<\nu_2\\ \nu_3<\nu_4}}\left(\begin{array}{l}(j_+)_{\nu_3\nu_2}(j_-)_{\nu_4\nu_1}-(j_+)_{\nu_4\nu_2}(j_-)_{\nu_3\nu_1}\\ +\,(j_+)_{\nu_4\nu_1}(j_-)_{\nu_3\nu_2}-(j_+)_{\nu_3\nu_1}(j_-)_{\nu_4\nu_2}\end{array}\right)\mathbf{a}^\dagger_{\nu_3}\,\mathbf{a}^\dagger_{\nu_4}\,\mathbf{a}_{\nu_2}\,\mathbf{a}_{\nu_1}. \tag{11}$$

These terms are known as "recoil" terms and usually are neglected, with the rationalization that the Nilsson model parameters have been adjusted to give the correct one-quasiparticle energy spectrum without them, and their inclusion would require some awkward readjustment in the shell-model potential. However, our reexamination showed that the recoil term makes a large off-diagonal contribution, reinforcing pairing matrix elements between high-j orbitals of projection Ω differing by 1. Furthermore, the separation between seniority-0 and seniority-2 states can be significantly affected. Thus, we chose to include diagonal and off-diagonal contributions of the $\mathbf{j}\cdot\mathbf{j}$ recoil terms for the $i_{13/2}$ neutron orbitals and $h_{11/2}$ proton orbitals and neglect it for the low-j orbitals. To include recoil terms for the low-j orbitals would add considerably to the computational time and was judged to be less important especially since our calculation excludes configurations with broken pairs in all but the highest-j orbital. In discussing the rotational Hamiltonian, the time-reversal basis for the single-particle orbital is not used but the phase conventions are kept consistent in our calculation.

TABLE II. Comparison of theoretical eigenvalues to the experimental energy levels.

	9 neutron levels (keV)		12 neutron levels (keV)		12 neutron levels (keV)		9 neutron and 9 proton levels (keV)		Expt. (keV)	
β_2	0.23		0.23		0.28		0.23			
I ($\hbar$)	Yrast	Yrare	Yrast	Yrare	Yrast	Yrare	Yrast	Yrare	Yrast	Yrare
0	0	714	0	756	0	1119	0	687	0	681
2	104	818	104	859	101	1212	112	801	123	816
4	340	1056	341	1095	332	1422	365	1058	371	1048
6	698	1414	700	1452	682	1734	745	1444	718	1366
8	1156	1870	1163	1910	1137	2112	1231	1934	1145	1756
10	1694	2394	1709	2441	1674	2462	1797	2490	1637	2194
12	2289	2901	2316	2972	2261	2751	2421	3026	2184	2622
14	2917	3263	2960	3331	2828	3135	3080	3424	2778	3028
16	3557	3613	3616	3663	3306	3696	3758	3817	3405	3491
18	4017	4195	4049	4254	3791	4325	4275	4441	4016	4087
20	4481	4806	4492	4850	4338	4972	4807	5113	4647	4782
22	4998	5394	4989	5420	4955	5642	5405	5783	5350	5520
24	5563	5993	5533	6003	5641	6351	6065	6478	6122	6294
26	6176	6624	6124	6617	6397	7109	6784	7216	6955	7056
28	6838	7298	6763	7273	7225	7925	7563	8007		
30	7552	8020	7452	7976	8128	8804	8405	8858		

It should be mentioned that in the combined proton and neutron calculation the proton and neutron motions are coupled through the "recoil" term. The coupling term comes from the fact that both the protons and the neutrons contribute to the total angular momentum. From Eq. (11), this can be written as follows:

$$\mathbf{H}_{jj}^{pn} = \sum_{\substack{\nu_1,\nu_3 \text{ for } p \\ \nu_2,\nu_4 \text{ for } n}} [(j_+)_{\nu_4\nu_2}(j_-)_{\nu_3\nu_1} + (j_-)_{\nu_4\nu_2}(j_+)_{\nu_3\nu_1}]\, \mathbf{a}^\dagger_{\nu_3}\, \mathbf{a}^\dagger_{\nu_4}\, \mathbf{a}_{\nu_2}\, \mathbf{a}_{\nu_1}. \quad (12)$$

For realistic calculations of the neutron (proton) system alone, it is clearly not correct to use a fixed moment of inertia for the core, since broken pairs are allowed only in the $i_{13/2}$ neutrons ($h_{11/2}$ protons). In particular, there will be higher-order alignment of the $i_{13/2}$ neutrons ($h_{11/2}$ protons) at the higher spins, leading to an effective decrease in the rotational energy constant $a_{\rm rot}$ at higher spins. Models with variable moments of inertia may give a more realistic description. Especially in the cases where neutron (or proton) systems were treated microscopically with the other type of nucleon system within the core rotor it was felt that a variable moment of inertia (VMI) was appropriate. An empirical expression is used where $a_{\rm rot}$ starts at a low-spin value that fits the lowest rotational band spacing in ^{154}Gd and saturates at half this value, which corresponds roughly to a rigid-body moment of inertia. This can be expressed as

$$a_{\rm rot}(I) = a_{\rm rot}(0)\{1+\exp[-a'_{\rm rot}I(I+1)]\}/2, \quad (13)$$

where the values of parameters $a_{\rm rot}(0)$ and $a'_{\rm rot}$ are adjusted for an overall fit to the backbending curve. The actual values of the parameters are given in Table I. Our later calculations (see Appendix B) of the neutron-only system used a nearly constant core moment of inertia, yielding a better fit to limiting high-spin values of the yrast kinetic moment of inertia

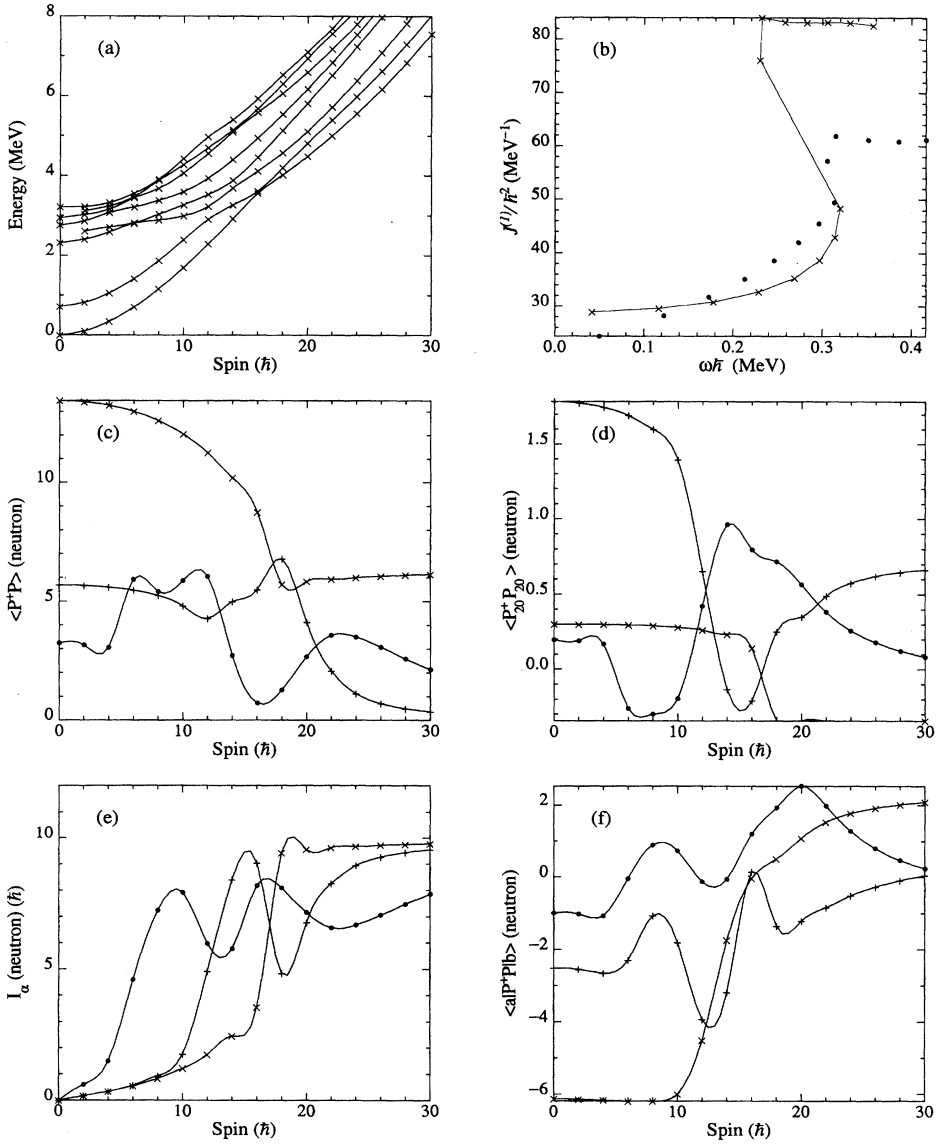

FIG. 1. Results for 12-neutron level calculation for ^{154}Gd with single-particle levels at the experimental ground $\beta_2 = 0.23$. (a) Lowest eight eigenvalues as a function of spin. (b) Plot of moment of inertia vs angular velocity from the yrast band. The dots are experimental values, and the solid curve is from the theoretical calculation. (c) The monopole pairing (without the diagonal contribution) expectation values for the lowest three bands. The symbols represent ×, yrast; +, yrare; ●, the second excited band. (d) Same as in (c) but for quadrupole pairing. (e) The spin alignment of the lowest three bands as a function of spin. The symbol are the same as in (c). (f) The monopole pairing matrix between two eigenstates as a function of spin. The symbols represent ×, yrast to yrare; +, yrast to the second excited state; ●, the yrare to the second excited state.

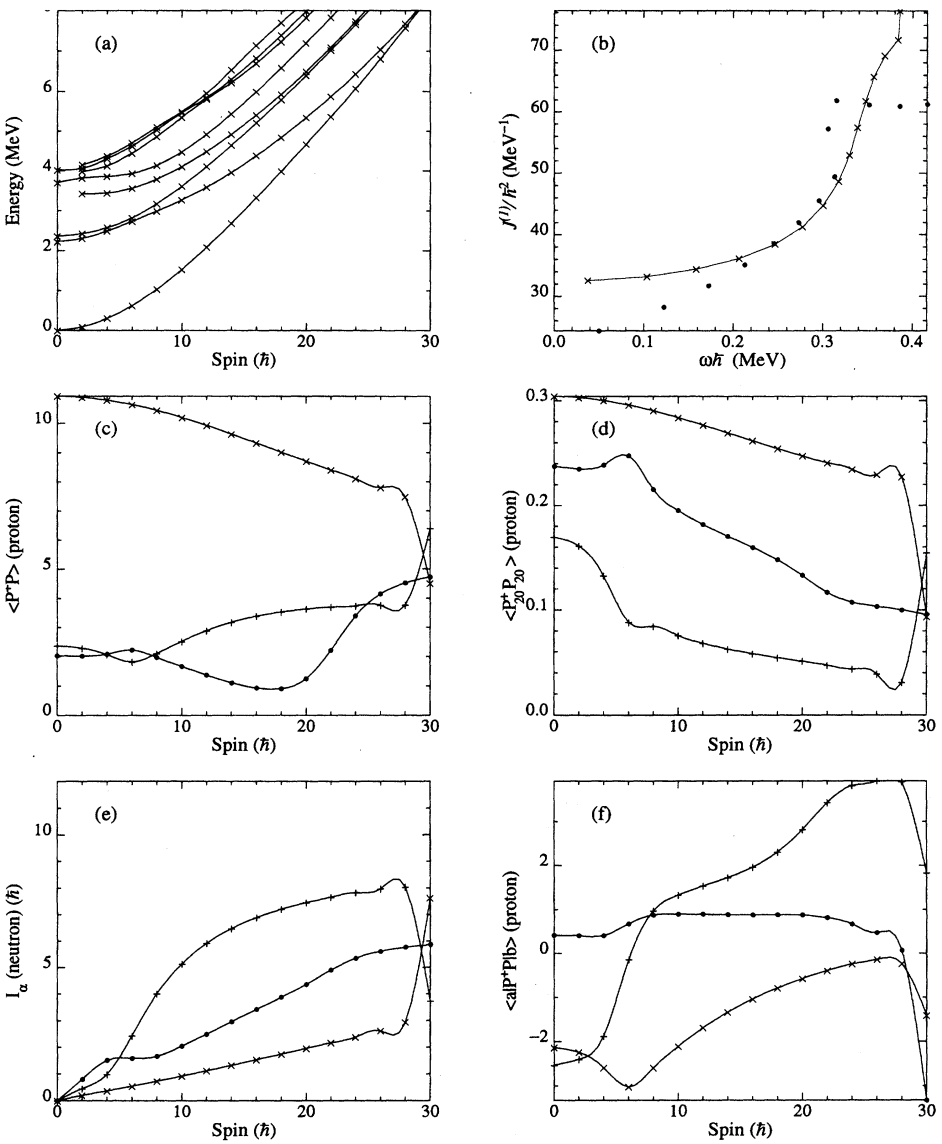

FIG. 2. Same as Fig. 1, except for results of the nine-proton levels calculation.

than did the variable expression (13). In retrospect the VMI feature of Eq. (13) might have been left out.

III. BASIS STATES AND SINGLE-PARTICLE ENERGIES

For exact matrix diagonalization (without the more common use of BCS variational approach) there is a combinatorial explosion in the dimensions as additional Nilsson orbitals are included in the basis. The dimensionality is easy to calculate for the constricted calculation of seniority-0 0^+ states and is just the binomial coefficient $\binom{N}{p}$, where N is the number of Nilsson orbitals and p is the number of nucleon pairs in the system. For the 9 orbitals and 4 or 5 pairs treated in Ref. [8] the matrix has the dimensions 126×126. For 40 orbitals and 20 pairs, comparable to the two-oscillator shells used in many BCS and Hartree-Fock-Bogolyubov (HFB) calculations, the dimensionality is close to Avogadro's number.

If broken pairs are included to treat nonzero spin, the dimensionality again climbs rapidly beyond practical limits even for supercomputers. Thus, just those broken pairs most important for moderate-spin rotational properties, including the aligned band and the backbending phenomena, are included.

Clearly, broken pairs in some $i_{13/2}$ neutron orbitals near the Fermi surface must be allowed in order to reproduce the aligned band. Indeed, with the two nearest orbitals one can reproduce the aligned band but not the total cancellation of mixing with ground at the diabolic point. For the latter, a minimum of the three nearest $i_{13/2}$ orbitals is required. Broken pairs in odd-parity neutron orbits which are of lower j are not allowed. Thus, their contribution to the moment of inertia enters only through the core moment of inertia. Most configurations with body-axis projection of angular momentum $K=$ 0, 1, and 2 are included. This paper presents results for the even-spin states of ^{154}Gd, but similarities to the even-even 90-neutron isotones are evident. The four $i_{13/2}$ orbitals included are the $\Omega=$ 1/2, 3/2, 5/2, and 7/2 projections. To limit the number of basis states, those with $K>2$ are ex-

cluded, since they will be coupled to the low-lying states only through higher-order Coriolis interactions and occur with higher single-particle energies.

With the above limitations, the dimensionality of the Hamiltonian matrix is 266×266 for 8 neutrons in 9 Nilsson orbitals, 3 of which are $i_{13/2}$. The dimensionality of the system with 12 neutrons in 12 Nilsson orbitals is 2646×2646. The matrix must be diagonalized for each spin value, which is done for even spins from 0 to $30\hbar$. Results for the 9-orbital neutron system and then for a 12-orbital neutron system at quadrupole deformations of 0.23 and 0.28 (with four $i_{13/2}$ orbitals and renormalized pairing strength) are presented in Table II in order to test convergence in these small basis calculations. Also, results for a combined 9-neutron and 9-proton orbital system are shown in Table II. In the latter case one has to diagonalize a $17\,527\times17\,527$ matrix. For this purpose, a modified version of a code obtained from H. Wildenthal, based on the LANCZOS algorithm was used.

IV. RESULTS FOR THE NEUTRON-ONLY AND PROTON-ONLY CALCULATIONS

It early became clear that the sharp experimental band crossing could not be reproduced with the energy levels from the deformed Woods-Saxon code at the theoretical equilibrium deformation values ($\beta_2=0.23$, $\beta_4=0.046$) of Nazarewicz [17]. The chemical potential for $N=90$ lies midway between the lowest two $i_{13/2}$ orbitals, giving a soft crossing. The most reasonable way to shift the chemical potential to near the $i_{13/2}$ ($\Omega=3/2$) orbital energy was to shift upward the energy of orbitals from the major shell below, namely, the $h_{11/2}$ neutron orbitals ($\Omega=9/2$ and $11/2$). There is some experimental justification for this because of the low-lying $11/2^-$ levels observed in adjacent odd-N nuclei.

We realized later that if we had used the somewhat larger β_2 deformation of 0.28 the arbitrary shift of $h_{11/2}$ neutron levels might not be necessary. Appendix B shows recalculations with single-particle energies at $\beta_2=0.28$. This might at first seem unreasonable in view of the Nazarewicz [17] theoretical calculations giving a $\beta_2=0.23$ close to the experimental β_2. The private communication from Nazarewicz gave indication of no beta stretching as the spin increased. Recently, at our request, Egido [18] has run his sophisticated Gogny-force nuclear structure code for ^{154}Gd with the result of β_2 near 0.28, with no beta stretching. This result is in disagreement with the lowest $2+\rightarrow0+$(ground) $E2$ strength. We have heard indirectly that there exists a theoretical shape calculation showing beta stretching from 0.23 near ground to 0.28 near first yrast band crossing. However, our literature search has failed to find such a study. It seems that all three deformation theory results are plausible, given the great sensitivity to input parameters at $N=90$, where there is a confluence of strongly deformation-driving orbitals of opposite type. A plot of experimental $B(E2)$ values vs spin, as given by Wollersheim and Elze [19] (their Fig. 2), shows clearly the departure of $B(E2)$ values from the fixed-deformation rotor for ^{154}Gd. We calculated the next three higher-spin points using lifetime data from the most recent Nuclear Data sheets. These points nicely follow the solid line and its extension, confirming beta stretching from spin 4 to 10.

We considered, but rejected, the idea of using a spin-dependent deformation, with a different single-particle level set for each spin. Even if the yrast deformation values were known experimentally or theoretically, the yrast deformation would not be the proper deformation for any excited states of a given spin, where relative populations of prolate-driving and oblate-driving orbitals changed. Furthermore, a deformation changing with spin would give nonorthogonalities of basis that would give serious problems in using the wave vectors for pair-transfer and electromagnetic transition probabilities in subsequent works. It is clearly appropriate to carry out the calculations for all spins using a set of single-particle energies calculated at a fixed deformation of the Woods-Saxon potential well. (One can expand in any basis, even spherical, but the expansion converges more rapidly in a deformed basis at the experimental deformation.) We will say more on this in Sec. VI and in Appendix B.

The lowest eight bands (neutron excitations) calculated for the ^{154}Gd 12-neutron orbital system for strong Y_{20} quadrupole pairing ($G_q/G_m\approx2.5$) and shift of $+1.55$ MeV for the $h_{11/2}$ neutron energy levels are shown in Fig. 1(a). The sharp yrast crossing at spin $(16-18)\hbar$ closely matches experiment, though the sharpness is very sensitive to the chemical potential in this model and the sharpness is tuned by shifting the $h_{11/2}$ orbitals up 1.55 MeV.

As a surprising bonus, the crossing of second and third bands around spin $12\hbar$, experimentally observed in ^{154}Gd, is reproduced. The traditional backbending plot is shown in Fig. 1(b), comparing theory with experiment. The expectation values of the monopole and quadrupole pairing terms for the lowest three bands are shown in Figs. 1(c) and 1(d), respectively. The monopole pairing expectation value, equivalent to the BCS $(\Sigma_i u_i v_i)^2$, is about 13.4 in the ground state, and it steadily decreases with spin, as expected due to the Coriolis antipairing (CAP) effect. We need to make clear that the $\langle\mathbf{P}^\dagger\mathbf{P}\rangle$ expectation values plotted in Figs. 1(c), 1(d), and 1(f) exclude diagonal terms $\mathbf{a}^+_\nu\,\mathbf{a}^+_{\bar\nu}\,\mathbf{a}_{\bar\nu}\,\mathbf{a}_\nu$, so as to vanish when there is no pairing correlation. This makes our plotted $\langle\mathbf{P}^\dagger\mathbf{P}\rangle$ equivalent to Δ^2 in BCS, but our values are no longer positive definite and are not directly comparable to the pair-transfer sum rules. The diagonal monopole terms of Eq. (3) are included in the Hamiltonian, though. The two excited bands have significantly lower monopole pairing correlations. The smooth trends apply to the extension of the bands beyond the sharp band crossing near spin $18\hbar$. In Fig. 1(d), the first excited band has the greatest quadrupole pairing expectation value at the bandhead, switching at the soft band crossing at spin $12\hbar$.

It was at first surprising that the Coriolis antipairing (CAP) effect is comparable to that in HFB calculations with a much larger shell-model space [20]. However, there are compensating features for CAP in our model, namely, that only 12 orbitals used might promote a more rapid pairing decrease, but the constraint that the 8 odd-parity orbitals may not have broken pairs has the opposite effect of slowing pairing collapse. It would be legitimate in our small-basis model to introduce a spin-dependent pairing force strength, but that does not seem to be necessary, at least in the 90-neutron region. Of course, at sufficiently high spin our exclusion of pair breaking in lower-j orbitals will result in too much pairing.

In Fig. 1(e), we show the neutron-aligned angular momentum i_α. These are not calculated from energy levels, as

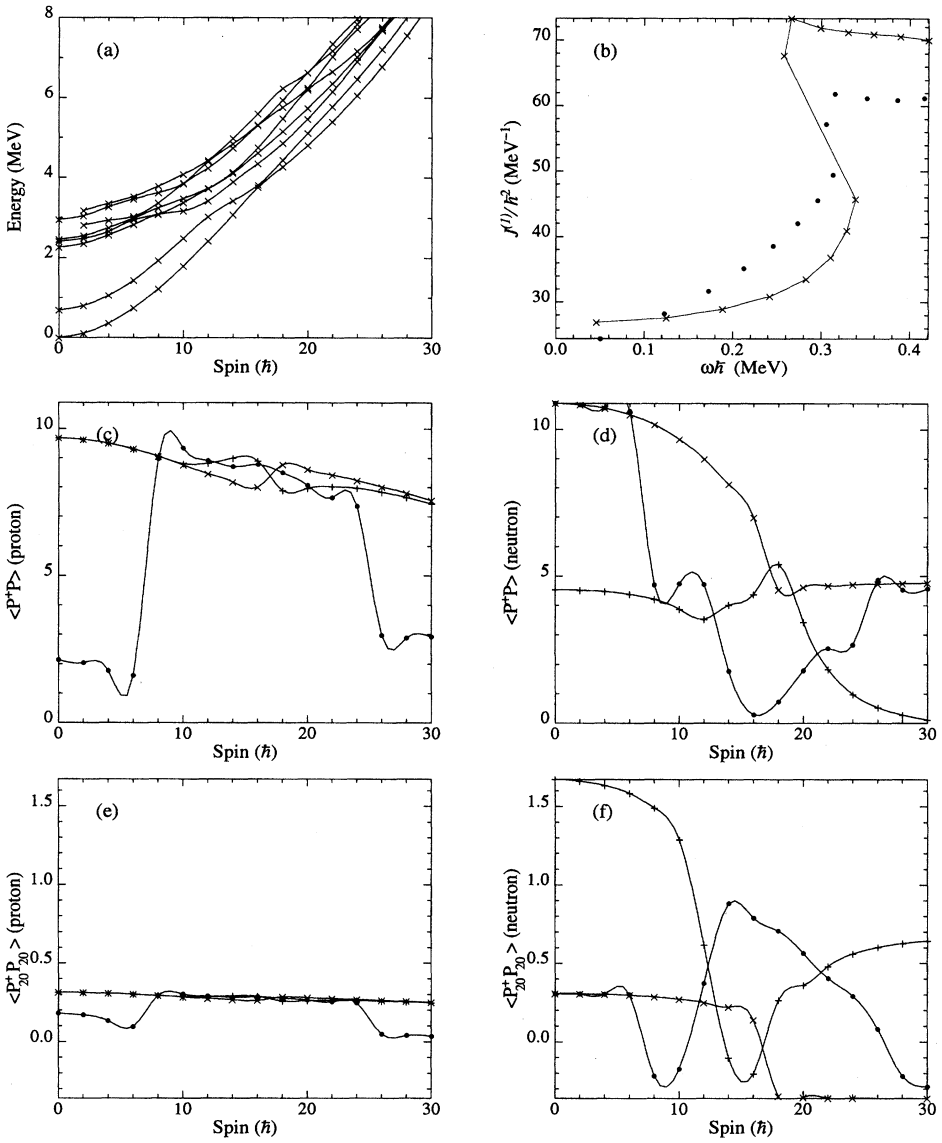

FIG. 3. Results for combined nine-neutron-level and nine-proton-level calculation for ^{154}Gd. (a) Lowest eight eigenvalues as a function of spin. (b) Plots of moment of inertia vs angular velocity from yrast band. The discrete dots are experimental values, and the solid curve is from theoretical calculation. (c) The proton monopole pairing (without the diagonal contribution) expectation values for the lowest three bands. The symbols represent $\times$, yrast, $+$, yrare, and $\bullet$, the second excited band. (d) Same as in (c) but for neutron monopole pairing. (e) Same as in (c) but for proton quadrupole pairing. (f) Same as in (c) but for neutron quadrupole pairing.

must be done with experimental data to infer spin alignment. Rather, these are microscopic expectation values calculated directly from the wave functions $\langle \mathbf{I}\cdot\Sigma\mathbf{j}\rangle/\sqrt{I(I+1)}$. From Fig. 1(a) there is no idealized aligned band (displaced parabola with minimum energy around i_α) as the calculations of Hara and Sun [14] have obtained. Rather, there seems to be a spin-aligned strength function which moves down into the yrare at spin $(14-16)\hbar$, and onto the yrast for spin $\gtrsim 18\hbar$. The alignment saturates at about $9.8\hbar$, quite comparable with the spin alignment deduced from energy levels by Morrison *et al.* [21].

An interesting and unexpected feature in Fig. 1(e) is that above band crossing ($I \gtrsim 18\hbar$) both yrast and yrare states have large and nearly identical neutron alignment (the conventional expectation is that yrare is a continuation of the ground band and would have low alignment). The story is revealed in Figs. 1(c) and 1(d). At highest spins the yrast and yrare differ in that the yrast exploits monopole pairing and the yrare the quadrupole pairing (just as at lowest spins). Their neutron alignment structures are the same. At highest spins, the strength of the ground band, with its low neutron alignment, is spread to yet higher states.

In Fig. 1(f), the off-diagonal elements of the monopole pairing operator among the three lowest states are plotted, ($\times$) first to second, ($+$) first to third, and ($\bullet$) second to third. The large magnitude (~ -6) of the first-to-second element signifies that the first excited state has pairing-vibrational strength through spin $10\hbar$, where it crosses the aligned band and changes character.

The corresponding HMD calculations are shown in Fig. 2 for the proton system with nine orbitals, three of which are $h_{11/2}$. Note in Fig. 2(a) that there is a sharp crossing of the yrast band, but not until spin $28\hbar$, considerably higher than the neutron band crossing of Fig. 1(a). The proton single-particle energies are bunched into three levels close to the Fermi energy. As a consequence, we see near-ideal pairing behavior at lower spins, with the pairing strength concentrating on yrast and the first two excited bands nearly degenerate

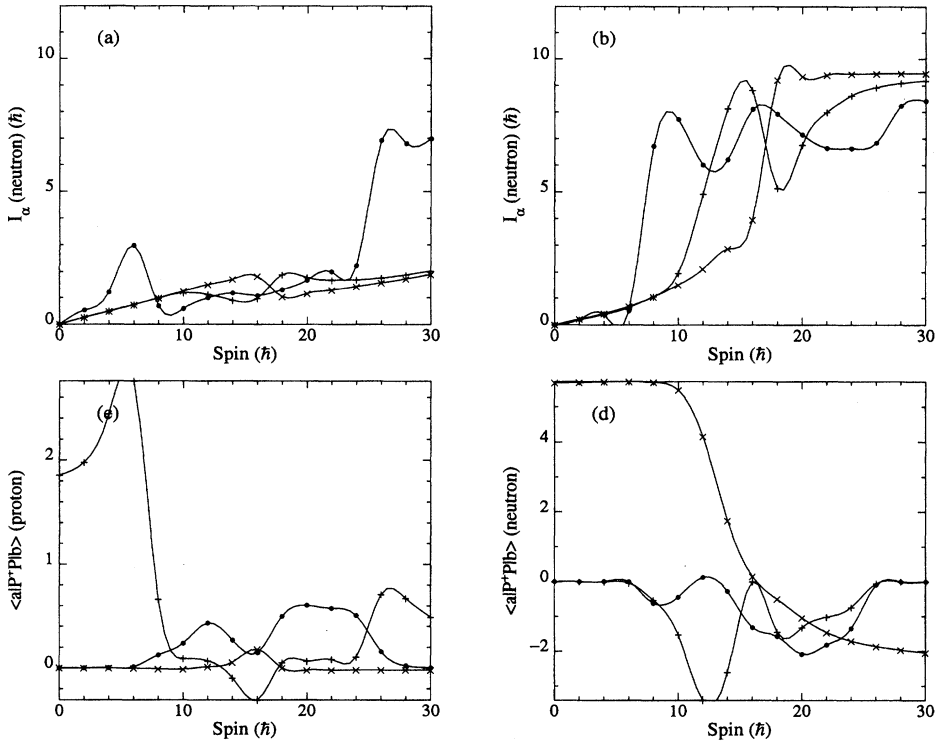

FIG. 4. Plots of spin alignments and off-diagonal monopole pairing matrix elements of the combined calculation for ^{154}Gd. (a) The proton spin alignment as a function of spin for the lowest three bands. The symbols represent ×, yrast, +, yrare, and ●, the second excited band. (b) Same as in (a) but for neutron spin alignments. (c) Proton monopole pairing matrix between two eigenstates as a function of spin. The symbols represent ×, yrast to yrare, +, yrast to the second excited state, and ●, the yrare to the second excited state. (d) Same as in (c) but for neutron monopole pairings.

and with little pairing. Past spin $8\hbar$ the yrare band takes on proton alignment character with i_α rising to around 8 at spin $28\hbar$, just before crossing the yrast. The quadrupole pairing correlation remains small, a consequence of there being little difference among the quadrupole moment values of the various proton orbitals. That is, for a system of Nilsson orbitals with nearly the same slope, quadrupole pairing only has the effect of a simple renormalization of monopole pairing.

V. RESULTS OF THE COMBINED PROTON-NEUTRON SYSTEM

Finally, a combined neutron-proton system with nine orbitals each was examined for ^{154}Gd. This combined system requires us to diagonalize a 17 527×17 527 matrix for each spin, necessitating several days of CPU time on a Sparcstation 2. The results are shown in Figs. 3 and 4. The lowest two bands change their behavior very little from the neutron-only calculation of Fig. 1. At the ~2.2 MeV bandhead of the neutron calculation of Fig. 1(a), there appear two additional nearly degenerate bands, which are obviously proton-excited bands, as shown in Fig. 2(a). Indeed, the second excited band is a proton excitation [see Fig. 3(c)] until a band crossing at spin $(6-8)\hbar$. The neutron pairing properties of the yrast and yrare are almost unchanged [see Figs. 3(c) and 3(d)] from the neutron-only calculation shown in Fig. 1.

Figure 4 shows (a) the spin alignment for protons, (b) the same for neutrons, and (c) and (d) the off-diagonal matrix elements for proton and neutron monopole pairing among the lowest three states. The neutron alignment is much the same as for the neutron-only calculations of Fig. 1 up to spin $26\hbar$, where a proton alignment character appears in the third bands of Fig. 3. From Fig. 4(a), we see that the third band takes on the character of proton alignment at spins of $\sim 26\hbar$ ($i_{\alpha p} \sim 7$), and the neutron alignments at these spins are high for all three lowest bands.

VI. DISCUSSION AND CONCLUSIONS

Largely motivated by the need for good sets of microscopic wave functions to use with neutron-pair-transfer reaction codes, we undertook multiparticle-plus-rotor calculations by exact diagonalization of large Hamiltonian matrices. Particularly inviting were the experimental ^{206}Pb + ^{156}Gd studies of Helmer *et al.* [22], which the measured rotational band population in neutron pair transfer in both directions. Thus, we needed microscopic wave functions of deformed Gd nuclei 154, 156, and 158. Although the combinatorial explosion of numbers of configurations for deformed rare-earth nuclei at first seemed daunting, it was our belief that essential properties of most of the low-lying states would be governed by the properties of the Nilsson orbitals lying near the Fermi energy within an energy interval of the pairing gap. We had been encouraged in that hope by the success in understanding (p,t) and (t,p) reaction strengths among 0^+ states of deformed rare-earth nuclei [23]. In our present study we went beyond that work on 0^+ states in that we departed from seniority zero and allowed broken pairs in the highest-j orbitals in a multiparticle-plus-rotor model. That made possible the calculation of rotational bands and indeed seems to capture the essential features of lower band crossings. Up to now we have not attempted to include odd-parity levels or any bands involving broken pairs in the lower-j orbitals. Furthermore, it is not expected that our codes, using at most 12 Nilsson orbitals about the Fermi energy, will be able to reproduce gamma-vibrational or octupole-vibrational bands,

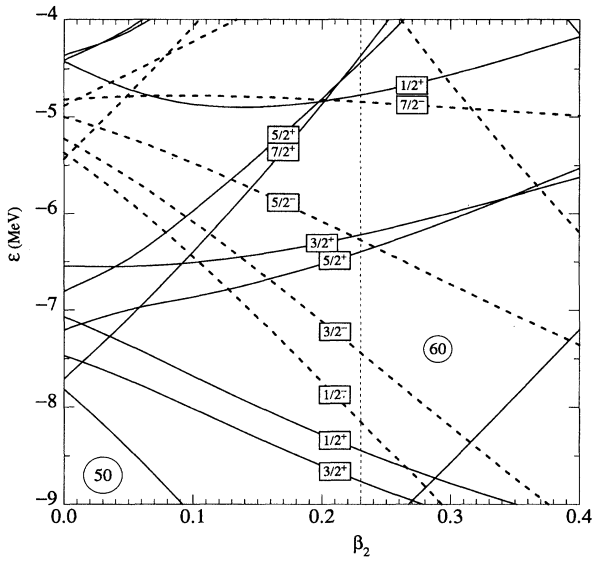

FIG. 5. The proton single-particle levels near the Fermi surface of ^{154}Gd are plotted as functions of the deformation β_2, with β_4 fixed at the constant value 0.046. The Ω quantum number labels the single-particle level, and the vertical dotted line indicates the location of the theoretical β_2 deformation for ^{154}Gd.

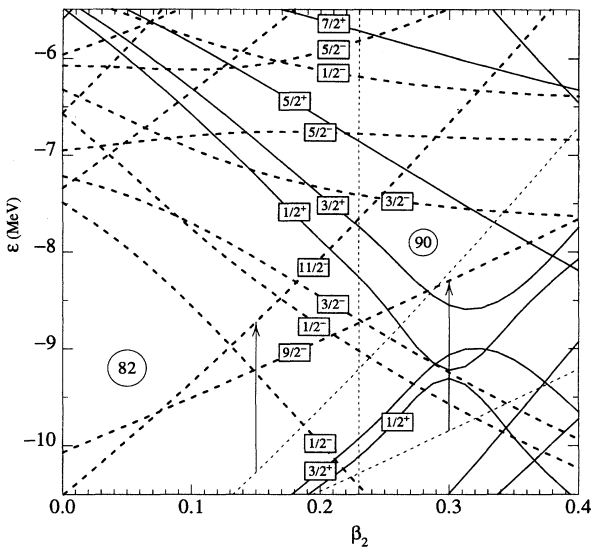

FIG. 6. Same as Fig. 6 but for neutrons. The energy of the $h_{11/2}$ orbitals (thinner-dotted lines) is shifted upward by 1.55 MeV as indicated by the vertical arrows.

which draw collective strength over a somewhat wider range of orbitals.

In our previous reports on Th isotopes 230, 232, and 234 [9] and on Dy isotopes 160, 162, and 164 [24] the calculations with basis states at fixed deformation are well justified, since the nuclei in question are well removed from the edge of the region of stable quadrupole deformation. That is not the case for the $N=90$ nuclei, such as ^{154}Gd, treated here. There are several papers on the possible shape coexistence in these nuclei, and there is clearly a softness toward quadrupole deformation. Nevertheless, we felt it important to try our fixed-basis model for ^{154}Gd, since the neutron-pair-transfer data we hoped to confront involved this nucleus and since the data on energy levels of the lowest three bands are so extensive.

Another reason that it is interesting to push the limits of our model at $N=90$ is that it is likely that nontrivial effects of quadrupole pairing may be observed. Well within the deformed region the Nilsson orbitals near the Fermi energy

TABLE III. Single-particle energies of basis states.

Proton		Neutron		
$N,j,^{a}\ \Omega^{\pm}$	Energy (MeV) $\beta_2=0.23$	$N,j,^{a}\ \Omega^{\pm}$	Energy (MeV) $\beta_2=0.23$	Energy (MeV) $\beta_2=0.28$
5, $\frac{11}{2}$, $\frac{1}{2}-$	−8.1467[b]	6, $\frac{13}{2}$, $\frac{1}{2}+$	−8.2798[b]	−8.9009
5, $\frac{11}{2}$, $\frac{3}{2}-$	−7.4402[b]	6, $\frac{13}{2}$, $\frac{3}{2}+$	−7.7491[b]	−8.2579
5, $\frac{11}{2}$, $\frac{3}{2}-$	−6.2766[b]	6, $\frac{13}{2}$, $\frac{5}{2}+$	−6.8544[b]	−7.1969
5, $\frac{11}{2}$, $\frac{7}{2}-$	−4.8438[b]	6, $\frac{13}{2}$, $\frac{7}{2}+$	−5.7172[b,c]	−5.8387
4, , $\frac{1}{2}+$	−8.4444	5, $\frac{11}{2}$, $\frac{9}{2}-$	−8.7317[d]	N.A.
4, , $\frac{3}{2}+$	−6.2217	5, $\frac{11}{2}$, $\frac{11}{2}-$	−7.6585[d]	−8.4563
4, , $\frac{5}{2}+$	−4.4359	5, , $\frac{1}{2}-$	−9.0213[c]	−9.3634
4, , $\frac{5}{2}+$	−6.3974	5, , $\frac{3}{2}-$	−8.7001	−9.0442
4, , $\frac{1}{2}+$	−4.7732	5, , $\frac{5}{2}-$	−6.7776	−6.7294
		5, , $\frac{3}{2}-$	−7.4088	−7.4201
		5, , $\frac{5}{2}-$	−5.8190[c]	N.A.
		5, , $\frac{1}{2}-$	−6.1870	−6.1413
		4, , $\frac{1}{2}+$	N.A.	−9.4013
		4, , $\frac{3}{2}+$	N.A.	−9.2085

[a]Approximate j quantum number.

[b]Intruder orbitals.

[c]Used only in 12-neutron-orbital calculation.

[d]Neutron $h_{11/2}$ orbital shifted by 1.55 MeV.

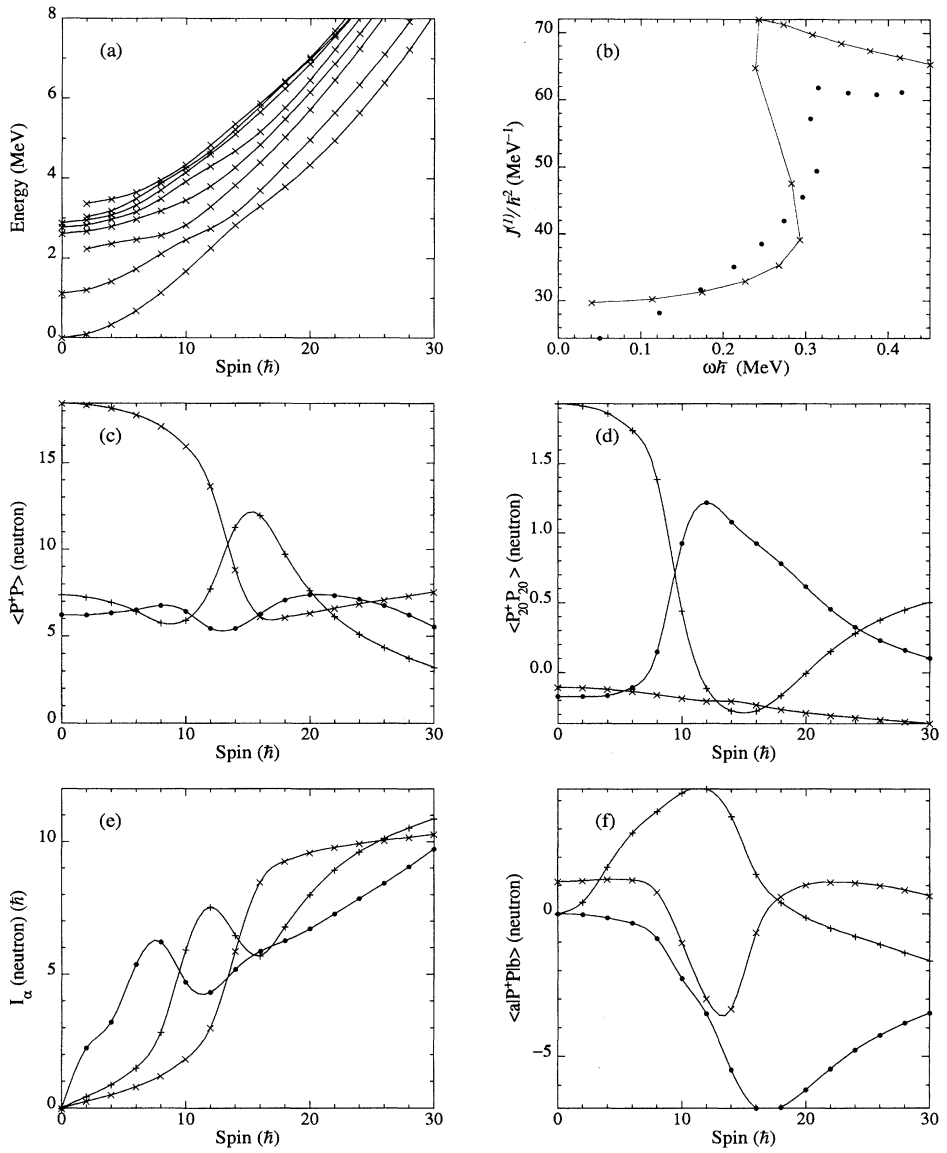

FIG. 7. Same as Fig. 1 except that these 12-neutron-orbital calculations were carried out for single-particle levels from larger $\beta_2 = 0.28$.

have generally similar slopes; that is, the mass quadrupole moments associated with various orbitals are similar. It is easy to show in such a case that the addition of a quadrupole pairing interaction effects just a trivial renormalization of the monopole pairing interaction. However, at the edge of deformation, where strong up-sloping (oblate-driving) and down-sloping (prolate-driving) orbitals are both near the Fermi energy, quadrupole pairing plays a special role. Whereas monopole pairing energetically favors coherent states with all the same sign for configurations with different arrangements of pair occupation, quadrupole pairing will favor a coherence with signs dependent on the signs of the orbital quadrupole moments. We indeed find a great sensitivity of the $N=90$ first excited $0+$ energy to the quadrupole pairing strength.

With the availability of greater computing power, it is now feasible to use more traditional shell-model approaches with large matrix diagonalization to model nuclear band structure. The insights gained from decades of pairing force BCS, random-phase-approximation (RPA), and HFB calculations form a strong guide from which one can now determine band structure by exact matrix diagonalization on basis sets of a few orbitals near the Fermi surface. The resulting HMD wave functions have good angular momentum and particle number and should provide wave functions valuable for theoretical studies on near-barrier heavy-ion inelastic scattering and transfer reactions [25].

ACKNOWLEDGMENTS

This work was supported by the Director of Energy Research, Division of Nuclear Physics of the Office of High Energy and Nuclear Physics of the U.S. Department of Energy, under Contracts DE-FG03-87ER40323, W-7405-

ENG48, and DE-AC03-76SF00098. One of the authors (J.O.R.) wishes to thank the Alexander von Humboldt Foundation for support of his work while at the Technical University of Munich in Garching. L.F.C. gratefully acknowledges travel support from the Brazilian-Conselho Nacional de Pesquisas e Desenvolvimento Científico (CNPq) under the U.S.-Brazil NSF-CNPq cooperative research grant INT-8382853. L.F.C. also acknowledges the hospitality and support of Nuclear Science Division at LBL during recent visits.

APPENDIX A: INPUT PARAMETERS

The single-particle Hamiltonian of Cwiok *et al.* [13] for the deformed Woods-Saxon potential, including quadrupole and hexadecapole deformations, is used. The code SWBETA was used to calculate single-particle energies ϵ. A portion of the single-particle energy levels around the Fermi surface as a function of β_2 is shown in Fig. 5, for protons ($Z=64$), and in Fig. 6, for neutrons ($N=90$). The calculations include a hexadecapole deformation of $\beta_4 = 0.046$ with positive-parity levels denoted by solid lines and negative-parity levels by dashed lines. The levels are labeled with the appropriate Ω^π quantum numbers. The vertical dashed line indicates the β_2 deformation from a self-consistent total Routhian surface (TRS) calculation of Nazarewicz [17] for ^{154}Gd (the minimum had deformation parameters of $\beta_2=0.23$, $\beta_4=0.046$). These deformation parameters were fixed for the HMD calculations, and since the experimental hexadecapole deformation is twice the theoretical value for ^{154}Gd, the theoretical value was used for consistency. The vertical arrows in Fig. 6 (the neutron calculation) indicate the magnitude of the shift of the $h_{11/2}$ orbitals (1.55 MeV) as discussed in Sec. IV of the main text. The dotted lines correspond to the unshifted position of the $h_{11/2}$ orbitals.

One can clearly see from Fig. 5, Fig. 6, and Table III that the basis includes orbitals that are down sloping with increasing β_2 deformation (namely, prolate driving) and up sloping with increasing β_2 deformation (namely, oblate driving). Note the splitting of the degeneracy of same-j orbitals at $\beta_2=0$ owing to the hexadecapole deformation included in the calculation. Also, at larger deformations $\beta_2\sim0.3$, note the strong interaction between the neutron $\frac{1}{2}$ and $\frac{1}{2}$ orbitals and the $\frac{3}{2}$ and $\frac{3}{2}$ orbitals, clearly indicating the mixing of the levels. The single-particle levels actually used in the calculations are shown in Table III. The four sets of input parameters used in the calculations are shown in Table I.

APPENDIX B: RECALCULATION AT LARGER DEFORMATION

As pointed out in Sec. IV, the calculations in the main body of this paper were performed with single-particle energy levels calculated at the experimental quadrupole deformation of $\beta_2=0.23$. It was necessary to make a large positive shift in energy levels for the $h_{11/2}$ orbitals from the shell below in order to reproduce a sharp yrast band crossing. As we discussed in Sec. IV, experimental $E2$ transition rates show that the deformation probably increases with spin, and a deformation of $\beta_2=0.28$ near the band crossing could make the arbitrary energy shift of $h_{11/2}$ unnecessary. In this appendix we show and discuss the results of HMD calculations at the larger deformation. Figure 7(a) shows the band-energy results and is to be compared with Fig. 1(a). Both calculations are for the neutron-only system with 12 orbitals (plus rotor). At the larger deformation the orbitals included in the 12-orbital set nearest the Fermi energy must be changed somewhat, as examination of the neutron level diagram of Fig. 6 makes clear. Two upgoing orbitals $\frac{1}{2}+$ and $\frac{3}{2}+$ from the fourth oscillator shell are included in the set at larger deformation, while the upgoing $\frac{9}{2}-$ from the $h_{11/2}$ is deleted, since it no longer gets the upward shift of 1.5 MeV. The higher of two 5/2 orbitals is also deleted. Note now the important fact that the unshifted $\frac{11}{2}-$ orbital crosses the downgoing $\frac{3}{2}+$ right at the Fermi energy. This circumstance of the Fermi energy being so close to an $i_{13/2}$ level, the $\frac{3}{2}+$, results in the relatively sharp first yrast band crossing. The backbending plot of Fig. 7(b) shows a somewhat better agreement with experiment for the new higher deformation calculations, but that is mainly because a more nearly constant rotor moment of inertia is used in the new calculations. The general patterns of bands and band crossings are very similar between the two calculations. Several details differ. The first bandhead of spin 2 occurs as the third excited 2^+ state in the first calculations and as the second excited 2^+ state in the newer calculations. At highest spin is a bunching of three lowest bands, while in the new calculations two lowest bands comprise the bunch. Examination of parts (c) and (d) of Fig. 7 shows the same qualitative behavior of the monopole and quadrupole pairing expectation values. The yrast levels (and their continuation after band crossing) in each case show strong monopole pairing, falling off with spin because of the Coriolis antipairing effect (CAP). The yrare levels in contrast show strong quadrupole pairing, also with a CAP decrease with spin. In part (e) we view similar neutron-spin-alignment patterns. Curiously, the off-diagonal matrix elements of the pair-transfer operator, part (f), seem quite different between the old and new calculations. Let us compare only the elements connecting ground and first excited bands (x), since as noted from the level diagrams (a) the second excited states

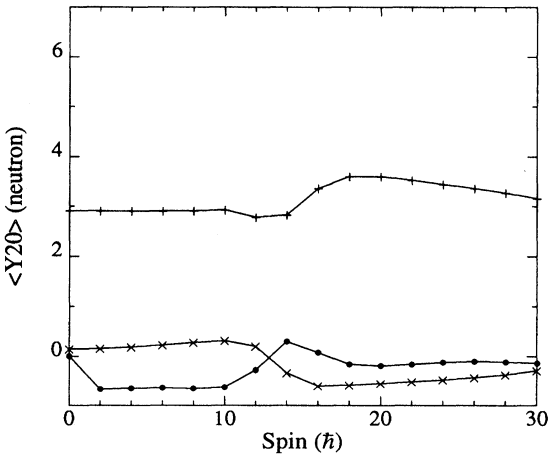

FIG. 8. Deformation-driving tendency of neutron systems in the three lowest bands, as a function of spin. The first excited band (+) is seen to be prolate driving throughout, and thus this band should be more prolate than the ground (×) and second excited band (●).

have a different character. In the old case there were strong pair-transfer matrix elements between the lowest two bands, up to spin 10, while in the new calculations these elements remain near zero up to spin 10. The off-diagonal pair-transfer matrix elements from yrast to higher bands are a measure of the "pairing vibrational" strength, and they will be sensitive to the presence of subshells in the single-particle spacing.

In Fig. 7(a) the energy of the first excited 0^+ is above 1 MeV, in disagreement with experiment for ^{154}Gd and other 90-neutron nuclei. Probably the inability of our model to calculate the first excited 0^+ state low enough at $N=90$ is a consequence of the beta softness at the edge of the deformed region. The $N=90$ nuclei are a challenge for our fixed deformation single-particle-energy basis. Our method, despite its lack of shape self-consistency, does give different mass quadrupole moments as the occupation probabilities of orbitals shift with increasing spin. The calculated mass quadrupole moments of the neutron system as a function of spin for the three lowest bands of Fig. 7 are shown in Fig. 8. The neutron system in turn will polarize the shape and modify the charge quadrupole moment. The prediction through spin 8 is that the first excited band is more prolate than the ground band. The experimental moments of inertia of these bands support that conclusion. Further, our model calculations suggest that the second excited band is the least prolate after the band-crossing region, where the deformation-driving tendencies of the neutrons converge, and deformations similar to the low-spin values prevail, with yrast and second excited bands reversing positions.

[1] A. Johnson, H. Ryde, and J. Sztarkier, Phys. Lett. B **34**, 605 (1971); A. Johnson, H. Ryde, and S. A. Hjorth, Nucl. Phys. **A179**, 753 (1972).

[2] B.R. Mottelson and J.G. Valatin, Phys. Rev. Lett. **5**, 511 (1960).

[3] F.S. Stephens and R.S. Simon, Nucl. Phys. **A183**, 257 (1972).

[4] R. Bengtsson, I. Hamamoto, and B. Mottelson, Phys. Lett. **73B**, 259 (1978).

[5] R.R. Hilton, H.J. Mang, P. Ring, J.L. Egido, H. Herold, M. Reinecke, H. Ruder, and G. Wunner, Nucl. Phys. **A366**, 365 (1981).

[6] T. Engeland, in Proceedings of the Nordic Winter School on Nuclear Physics, 1983 (unpublished), p. 155; also T. Engeland, Phys. Scr. **25**, 467 (1982); T. Engeland, A. Herriquez, and J. Rekstad, Phys. Lett. B **120**, 19 (1983).

[7] H.J. Mang, J.O. Rasmussen, and M. Rho, Phys. Rev. **141**, 941 (1966).

[8] A.A. Shihab-Eldin, J.O. Rasmussen, and M.A. Stoyer, *Proceedings of the Microscopic Models in Nuclear Structure Physics*, Oak Ridge, 1988 (World Scientific, Singapore, 1988), p. 282.

[9] S.Y. Chu, J.O. Rasmussen, R. Donangelo, M.A. Stoyer, S. Frauendorf, and Y.R. Shimizu, in *Proceedings of the Conference on Nuclear Physics in Our Times*, Sanibel Island, FL, 1992, edited by A. V. Ramayya (World Scientific, Singapore, 1993), p. 181.

[10] S.Y. Frank Chu, Ph.D. thesis, Yale University, 1993.

[11] P. Ring and P. Schuck, *The Nuclear Many-Body Problem* (Springer-Verlag, Berlin, 1980).

[12] R.R. Chasman, Phys. Rev. C **14**, 1935 (1976).

[13] S. Cwiok, J. Dudek, W. Nazarewicz, J. Skalski, and T. Werner, Comput. Phys. Commun. **46**, 379 (1987).

[14] K. Hara and Y. Sun, Z. Phys. A **339**, 15 (1991); Y. Sun, Ph.D. thesis, TU-München, 1991.

[15] I. Hamamoto, Nucl. Phys. **A232**, 445 (1974).

[16] A. Bohr, Mat. Fys. Medd. Dan. Vid. Selsk. **26**, 14 (1952).

[17] W. Nazarewicz (private communication). See also the closely similar ground state deformation values in W. Nazarewicz, M.A. Riley, and J.D. Garrett, Nucl. Phys. **A512**, 61 (1990).

[18] J.L. Egido (private communication).

[19] H.J. Wollersheim and Th.W. Elze, Nucl. Phys. **A278**, 87 (1977).

[20] M.L. Cescato, Y. Sun, and P. Ring, Nucl. Phys. **A553**, 455 (1991).

[21] J.D. Morrison, J. Simpson, M.A. Riley, P.D. Forsyth, D. Howe, and J.F. Sharpey-Schafer, J. Phys. G **15**, 1871 (1989).

[22] K.G. Helmer, C.Y. Wu, D. Cline, A.E. Kavka, W.J. Kernan, E.G. Vogt, M.W. Guidry, X.L. Han, R.W. Kincaid, X.T. Liu, H. Schecter, J.O. Rasmussen, A. Shihab-Eldin, M.A. Stoyer, and M.L. Halbert, Phys. Rev. C **48**, 1879 (1993).

[23] A.A. Shihab-Eldin, J.O. Rasmussen, M.A. Stoyer, D.G. Burke, and P.E. Garrett, Int. J. Mod. Phys. E **4**, 411 (1995).

[24] J.O. Rasmussen, L.F. Canto, S.Y. Chu, R. Donangelo, and M.A. Stoyer, in Proceedings of the Conference on Harmony in Physics, honoring S.T. Belyaev, University of Pennsylvania, Philadelphia, 1994 [Phys. Rep. (to be published)].

[25] S. Y. Chu, J. O. Rasmussen, M. A. Stoyer, L. F. Canto, R. Donangelo, and P. Ring, Phys. Rev. C **52**, 685 (1995).